Magnetic Resonance Spectroscopy Studies of Human Metabolism

Douglas E. Befroy[1,2] and Gerald I. Shulman[2,3,4]

Magnetic resonance spectroscopy (MRS) is a companion technique to the more familiar magnetic resonance imaging (MRI) scan. Whereas MRI determines the spatial distribution of water (and lipid) protons across a region of interest, MRS measures the chemical content of MR-visible nuclei, which include the metabolically relevant elements of hydrogen (^{1}H), carbon (^{13}C), and phosphorus (^{31}P). MRS is particularly advantageous for assessing metabolism because the chemical properties and environment of each nucleus determine the frequency at which it appears in the MR spectrum, giving rise to peaks corresponding not only to specific metabolites but also to the constituent nuclei of each metabolite (Fig. 1). It is therefore a multimodal, noninvasive technique capable of measuring a broad range of biological compounds across a variety of tissues. Repeated measures of metabolite content, metabolic fluxes, and their response to an intervention are possible, characteristics that make MRS ideally suited for in vivo studies of human metabolism. An additional advantage is that MRI scans can be obtained concurrently to provide structural/anatomical information that can guide data acquisition and assist in data analysis and interpretation. In this review, we will highlight some of the applications by which MRS can be used to investigate metabolism, focusing on its application to in vivo human studies.

METHODOLOGICAL CONSIDERATIONS FOR IN VIVO STUDIES

The versatility of MRS provides a hugely flexible technique capable of probing a broad range of metabolic applications across a variety of tissues. Despite its many advantages, particularly for studies of human metabolism where noninvasive techniques are at a premium, effective implementation of MRS in vivo requires consideration of its methodological limitations and how they influence its application in specific organs. In many instances, these issues can be overcome by the methodological setup and a judicious choice of the pulse sequence used to excite and detect the MR signal.

From the [1]Department of Diagnostic Radiology, Yale University School of Medicine, New Haven, Connecticut; the [2]Department of Internal Medicine, Yale University School of Medicine, New Haven, Connecticut; the [3]Department of Cellular and Molecular Physiology, Yale University School of Medicine, New Haven, Connecticut; and the [4]Howard Hughes Medical Institute, Yale University School of Medicine, New Haven, Connecticut.
Corresponding author: Douglas E. Befroy, douglas.befroy@yale.edu, or Gerald I. Shulman, gerald.shulman@yale.edu.
Received 19 June 2009 and accepted 29 January 2011.
DOI: 10.2337/db09-0916

As an analytical technique, MR is relatively insensitive compared with other modalities, and tissue metabolite concentrations in the millimolar range are required, generally, to be detectable in vivo. The low natural abundance of some MR-visible isotopes (e.g., ^{13}C is only 1.1% of total carbon) may further compromise detection, resulting in long scan times. Maximum sensitivity can be achieved by using an appropriate radiofrequency (RF) coil for signal detection, optimized for the nucleus of interest. Resonances of highly abundant compounds will dominate the spectrum and may obscure or distort peaks of interest. Water is an overwhelming signal in the ^{1}H spectrum of most tissues; ^{1}H and ^{13}C spectra of muscle and liver feature prominent lipid peaks. Because numerous peaks are observed in ^{1}H and ^{13}C spectra, spurious signals of other species, or unwanted signal infiltration from surrounding tissues (e.g., subcutaneous fat, the scalp), may overlap peaks of interest and impair the ability to resolve or quantify a particular metabolite.

Pulse sequences are available that suppress specific peaks (e.g., water suppression) (Fig. 2), that excite only resonances of interest, or that confine the MR signal to a specific volume (voxel), creating a localized spectrum (Fig. 3). Spectra can also be simplified by removing ("decoupling") the dipolar coupling interaction between adjacent nuclei (e.g., ^{13}C bonded to ^{1}H), which causes peak splitting, or by spectral "editing" to selectively enhance the signal from the metabolite(s) of interest. Typically, several of these options are combined to generate the best quality in vivo spectrum.

The MR properties of a compound or tissue may also modulate the extent to which a metabolite is visible or resolvable in vivo. Large proteins and macromolecules give rise to broad, nonspecific signals (visible as baseline distortions in brain ^{1}H spectra), and metabolite signals from liver and adipose tissue are significantly broader than those from muscle and brain because of the shorter T_2 relaxation times in these tissues. Spectral resolution is also compromised by effects that perturb the homogeneity of the local magnetic field within the region of interest; this is particularly apparent at air-tissue-bone interfaces (e.g., the sinuses), which exhibit differences in magnetic susceptibility. Resolution can be enhanced by correcting local field inhomogeneities by applying additional external magnetic-field gradients across the region of interest ("shimming").

All MR techniques are susceptible to artifacts induced by motion, whether a result of inadvertent movement of the subject, respiration, the cardiac cycle, or skeletal muscle contractions. These include the infiltration of unwanted regions into the volume of interest (e.g., the gall bladder during liver MRS), compromised voxel selection, and the blurring of spectral resolution. Breath hold is a common strategy during torso and abdominal MRI, but the longer acquisition times associated with MRS favor respiratory gating, typically at end expiration when chest

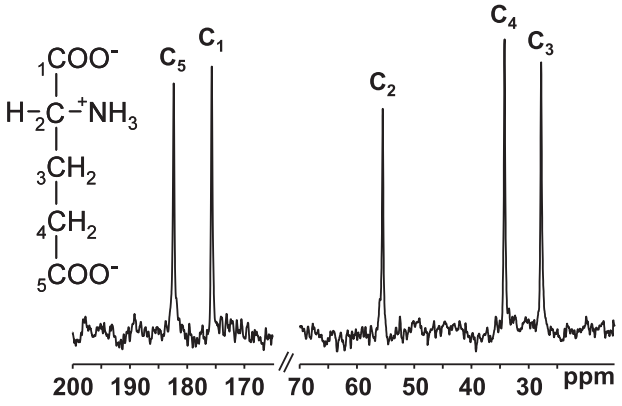

FIG. 1. MRS measures the chemical content of MR-visible nuclei across a region of interest and provides positional information as well as content. The ^{13}C-MRS spectrum of glutamate displays peaks corresponding to each carbon atom of the molecule.

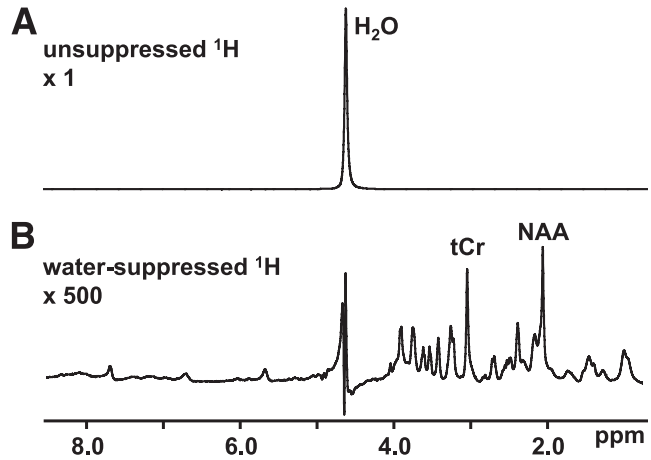

FIG. 2. In vivo MR spectra are dominated by signals from highly abundant metabolites. *A*: The ^{1}H spectrum of the brain features a prominent water peak that overwhelms the metabolite signals. Pulse sequences are available that selectively suppress or excite specific frequencies. *B*: The inclusion of a water-suppression module selectively minimizes the $^{1}H_2O$ peak and enhances the detection of brain metabolites. tCr, creatine-CH_3.

movement is minimal. MRS of the heart is typically accomplished with combined heart-rate and respiratory gating to compensate for both cardiac and respiratory motion. Although gating increases the experimental duration, the improvement in spectral quality is significant. Blood also is a major contaminant for cardiac MRS, and techniques have been developed to remove or correct for signal infiltration or artifacts induced by blood flow.

A detailed analysis of MRS pulse sequences, hardware, and techniques is beyond the scope of this review, but thorough descriptions can be found in the excellent book by de Graaf (1).

IN VIVO MRS STUDIES OF HUMAN METABOLISM

In vivo studies of human metabolism can be loosely grouped into four categories: *1*) static estimates of metabolite content (e.g., to examine a particular subject population or the effects of an intervention); *2*) dynamic monitoring of metabolites to investigate the effects of an intervention (e.g., exercise, insulin stimulation) in real time; *3*) calculation of unidirectional metabolic fluxes of equilibrium exchange reactions by magnetization transfer techniques; and *4*) estimation of metabolic reaction rates using MR-visible tracer kinetics. The following section will give a broad overview of the application of these techniques to investigate human metabolism in vivo.

Static measures of metabolite content. The most widely implemented in vivo MRS technique is the use of localized ^{1}H spectroscopy to estimate lipid content. In muscle, intramyocellular lipid (IMCL) and extramyocellular lipid (EMCL) peaks can be resolved (Fig. 3) as a result of slight differences in chemical shift between each compartment, an effect dependent on the relative orientation of the muscle fibers with respect to the field of the MR scanner (2). As a result of variations in composition, lipid content typically is expressed relative to the water or creatine peak used as internal standards. Extending initial findings in muscle biopsy studies, IMCL content was observed to be inversely correlated with insulin sensitivity in lean, healthy individuals (3) as well as in obese and type 2 diabetic subjects (4–6), suggesting a role for the accumulation of lipid in the mechanism of insulin resistance (7,8). A notable exception occurs in endurance-trained athletes, who have increased IMCL content despite remaining highly insulin sensitive (6), although this apparent paradox may be explained by enhanced conversion of detrimental lipid intermediates (e.g., diacylglycerol, ceramides) to triglyceride (TG) (9,10).

Analogous ^{1}H-MRS techniques can measure intrahepatic lipid (IHL), which has similarly been correlated with liver insulin resistance (8,11,12). Interventions that decrease IHL, including drug treatment (12–14) and diet and exercise (15–17), significantly improve hepatic insulin sensitivity. These methods are the first MRS techniques to achieve widespread implementation because data acquisition and analysis are relatively rapid (<1 h to measure both IMCL and IHL) and can be performed on clinical MR scanners. Our group now includes ^{1}H-MRS lipid measurements as a screening tool to help identify insulin-resistant individuals, and the techniques are also being used as a biomarker to assess the efficacy of lifestyle intervention in the TuLIP (Tuebingen Lifestyle Intervention Programme) trial (15,18). MRS estimates of IHL also have become the gold standard for the diagnosis of nonalcoholic fatty liver

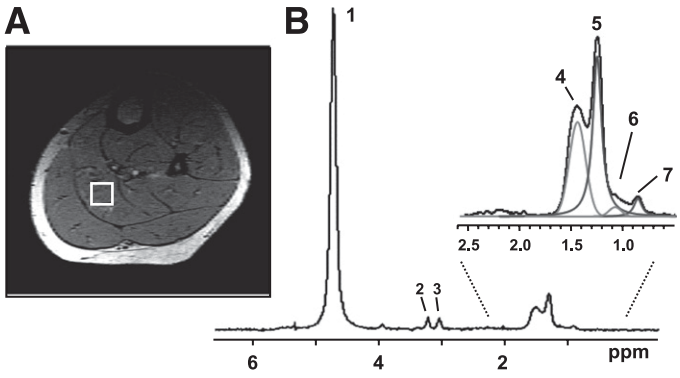

FIG. 3. A localized muscle ^{1}H spectrum acquired from a specific region (voxel) within the soleus muscle. *A*: The selected voxel is outlined by a white box superimposed on a cross-sectional MRI image of the calf. *B*: Multiple lipid peaks can be resolved enabling the quantification of IMCL and EMCL. Peak 1: water; peak 2: choline-CH_3; peak 3: creatine-CH_3; peak 4: EMCL-CH_2; peak 5: IMCL-CH_2; peak 6: EMCL-CH_3; and peak 7: IMCL-CH_3.

disease and steatohepatitis and have revealed interesting ethnic differences in the prevalence of fatty liver (19,20).

The presence of myocardial TG also can be observed using cardiac and respiratory-gated localized ^{1}H-MRS (21). Their accumulation has been correlated with BMI (22) and impaired glucose tolerance, occurring prior to the onset of overt type 2 diabetes or left ventricular systolic dysfunction (23).

The bioenergetic state of a tissue can be characterized by using ^{31}P-MRS to estimate the concentrations of high-energy phosphate (HEP) compounds or, more typically, their ratios. Unlike biochemical assays, only metabolically active (unbound) molecules are measured. Gross differences in muscle fiber–type composition can be distinguished on the basis of HEP ratios (24), and abnormalities also are observed in dystrophic muscle (25). The phosphocreatine (PCr)-to-ATP ratio is decreased in many cardiac disorders, including dilated cardiomyopathy, left ventricular hypertrophy, coronary artery disease, and heart failure, as well as infarcted heart (26–28). Bioenergetic deficits may predict clinical severity (27,29,30) and are accompanied by decreased creatine content, determined by ^{1}H-MRS (31), which also characterizes nonviable postischemic myocardium (32). Despite normal left ventricular morphology, mass, and systolic function, diabetic heart exhibits a decreased PCr-to-ATP ratio, which is associated with underlying diastolic dysfunction (33). Hepatic HEPs also can be measured, and decreases in ATP and inorganic phosphate (P_i) have been observed in nonalcoholic steatohepatitis (34) and type 2 diabetes (35), suggesting that impairments in liver energetics may be associated with the development of steatosis. Phosphoesters are detected in hepatic ^{31}P spectra, and alterations in phosphomonester and phosphodiester content have been observed in diffuse liver disease (36). Increases in the phosphomonester-to-phosphodiester ratio may be correlated with the severity of disease (37,38), enabling ^{31}P-MRS to offer an alternative to histopathology for assessing progression from steatosis to fibrosis to cirrhosis and hepatitis.

Edited and nonedited ^{1}H-MRS techniques also have been used to observe the effects of cerebral disease on brain metabolite content. Lactate content is elevated in infarcted regions following a stroke, whereas the neurologic marker *N*-acetyl aspartate (NAA) is decreased (39). Decreases in NAA have been detected in epileptogenic regions of the brain, with colocalized derangements in HEP content, suggesting that mitochondrial loss and a bioenergetic deficit may be a contributing factor (40). The inhibitory neurotransmitter, γ-aminobutyric acid (GABA), also is decreased in epileptic subjects and can be restored by Vigabatrin treatment (41), accompanied by a reduction in seizure occurrence (42).

Dynamic metabolic MRS. The classic dynamic MRS experiment is to monitor the bioenergetic response of ^{31}P metabolites to a sustained muscle contraction or exercise. To maintain the intracellular ATP concentration during this increased energy demand, PCr is depleted, P_i accumulates, and intracellular pH may also be modulated as a result of anaerobic glycolysis (Fig. 4). Although the intracellular concentration of free (unbound) ADP is too low to be observed directly with ^{31}P-MRS, it can be calculated indirectly, assuming equilibrium at creatine kinase (CK). Upon cessation of exercise, each metabolite recovers to baseline levels. With relatively rapid (<~8 s) time resolution and certain assumptions, a range of bioenergetic fluxes can be determined from the metabolite changes, including the CK flux and glycolytic and oxidative contributions to ATP production. A functional estimate of mitochondrial oxidative capacity can be calculated from the kinetics of PCr recovery. A detailed analysis of these methods is beyond the scope of this article, but several comprehensive reviews are available in the literature (43).

Several studies have investigated the energetic response of muscle to different workloads and conditions to examine the regulation of muscle energy production during exercise. Significantly, these studies have illustrated that PCr recovery kinetics are dependent not only on the end-exercise concentrations of PCr and ADP but also on pH (44). Therefore, to estimate mitochondrial capacity accurately, particularly when assessing populations with impaired muscle bioenergetics, these factors must be considered and controlled. MRS studies have demonstrated

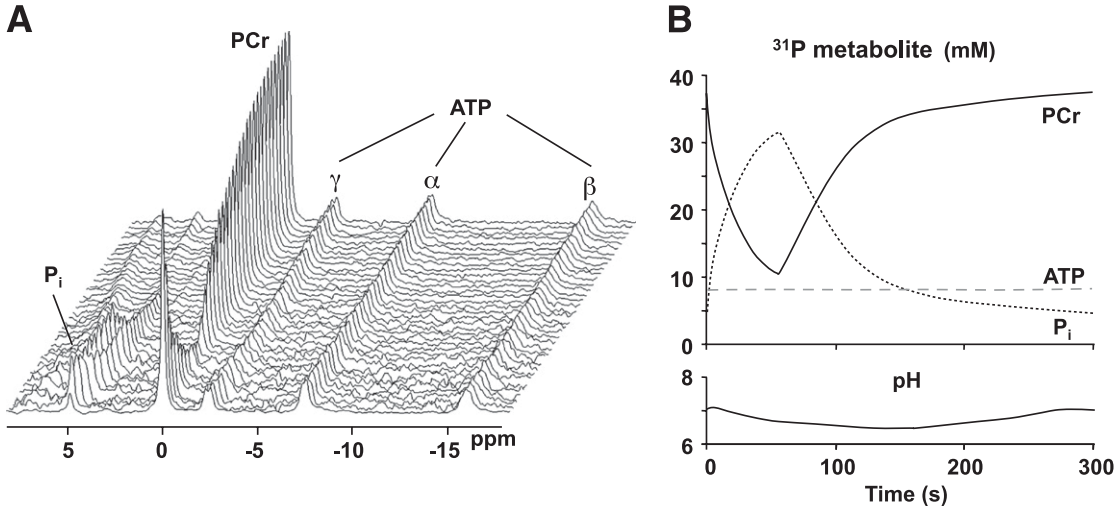

FIG. 4. *A*: Dynamic ^{31}P-MRS data acquired during muscle contraction and recovery (data courtesy of J. Kent-Braun). *B*: To maintain cellular ATP concentrations (dashed line) during the contraction, PCr (solid line) is depleted because of the CK reaction and P_i (dotted line) accumulates. Intracellular pH, calculated from the chemical shift separation between the PCr and P_i peaks, increases initially as a result of PCr hydrolysis; H+ production attributed to anaerobic glycolysis may cause intracellular acidification during longer contraction protocols. PCr, P_i, and pH recover to baseline upon cessation of the contraction.

that muscle oxidative capacity is increased by endurance training, consistent with mitochondrial biogenesis and enhanced aerobic performance, and that the metabolic perturbations associated with exercise are attenuated (45). The metabolic economy of muscle contraction during exercise has been found to decrease as intensity increases (46). During a ramped exercise protocol, elderly subjects exhibit less muscle acidification and are more resistant to fatigue (47), potentially as a result of less reliance on glycolytic ATP production and an undiminished mitochondrial oxidative capacity (48). Bioenergetic insufficiencies in muscle also have been observed in patients with cardiovascular disease (49,50), chronic fatigue (51), and type 2 diabetes (52). Dynamic ^{31}P-MRS may emerge as a clinical test for the early diagnosis of ischemic heart disease because abnormal cardiac energetics are observed in response to a handgrip exercise stress test (53,54), an effect that is apparent in the absence of angiographically significant coronary stenoses (55).

Myocellular oxygenation can be assessed using ^{1}H-MRS to monitor the appearance of deoxymyoglobin (oxymyoglobin is effectively undetectable) when a mismatch occurs between oxygen demand and supply (56) (e.g., during exercise or ischemia). The appearance of deoxymyoglobin in exercising muscle is approximately proportional to the workload at low to intermediate intensities and then reaches a plateau (57). Intracellular oxygenation is dependent on contraction frequency as well as intensity (58), and perfusion insufficiencies can be detected in peripheral artery disease (59). Lactate production in exercising muscle, attributed to anaerobic glycolysis, can be indirectly estimated from rates of intracellular acidification. Direct measurements of lactate using edited ^{1}H-MRS are possible in muscle (60,61), although they remain to be fully validated. In contrast, transient increases in brain lactate during photic stimulation can be directly observed using ^{1}H-MRS because of the lack of overlapping lipid peaks (62).

Intramuscular glycogen stores can be detected with ^{13}C-MRS and are depleted by longer-duration exercise (63); repletion occurs via insulin-dependent and independent mechanisms (63) and is influenced by diet (64). IMCL utilization also may occur, dependent on exercise duration and workload (65). The transition between the fed and fasting states has also been investigated using MRS techniques. During short-term fasting, liver glycogen is depleted (66), followed at longer durations (>72 h) by significant accumulation of IMCL (67) and IHL (68), which is likely driven by the increase in circulating plasma fatty acid concentrations. Postprandially, glycogen is replenished in muscle and liver (69) by both direct and indirect pathways of glycogen synthesis (70,71). Using a combination of MRS and non-MRS techniques, the contribution of hepatic gluconeogenesis to endogenous glucose production was estimated to be ~50%, even during the earliest time points of a fast, which is significantly higher than expected (66,72). In type 2 diabetes, elevated rates of fasting endogenous glucose production were found to be caused by increased gluconeogenesis rather than net hepatic glycogenolysis (73).

Magnetization-transfer techniques. The unidirectional fluxes that contribute to metabolic exchange reactions can be examined using magnetization-transfer (MT) techniques. The underlying concept of these methods is that if the MR signal of a metabolite is perturbed, the transfer of this effect to its exchange partner can be detected, with the magnitude of the MT effect proportional to the kinetics of exchange (Fig. 5). Unidirectional metabolic fluxes can then be calculated using classical reaction kinetics. Bioenergetic rates can therefore be investigated using ^{31}P-MT spectroscopy. Decreased CK (PCr → ATP) flux is observed in congestive heart failure (74) and left ventricular hypertrophy (75), suggesting that myocardial ATP generation is impaired in the pathophysiology of human heart disease. Rates of P_i → ATP flux have been estimated in resting muscle and were observed to be decreased in insulin-resistant elderly individuals (76) and insulin-resistant offspring of type 2 diabetic patients (77), indicating a bioenergetic deficit in these individuals. In contrast, in endurance-trained muscle, characterized by enhanced mitochondrial content and oxidative capacity, this basal flux is unchanged (78). Feasibility studies in human visual cortex (79) and, more recently, liver (80) also have been demonstrated. It is worth noting that high signal/noise spectra are required to accurately estimate the MT effect and that if the observed metabolite is involved in multiple exchange reactions more complex kinetic models and multiple-site MT methods are required (e.g., to measure ATP utilization). Finally, MT techniques estimate the total flux from all cellular contributions to a specific reaction, including futile cycling. These effects may lead to overestimation of the absolute

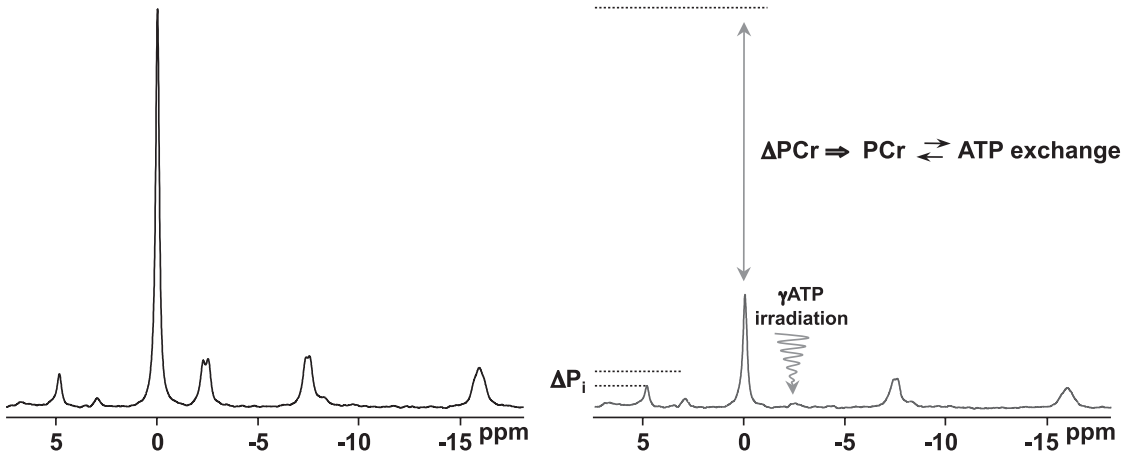

FIG. 5. Unidirectional fluxes attributed to chemical exchange can be measured using MT techniques. Application of ^{31}P saturation-transfer MRS in muscle: frequency-selective irradiation of the γATP peak causes reductions in the magnitude of the PCr and P_i peaks as a result of PCr ⇆ ATP (CK) and P_i ⇆ ATP (ATP synthesis/hydrolysis) exchange, respectively.

$P_i \rightarrow$ ATP flux in muscle (81) and complicate the interpretation of fluxes in liver, where the contributions of nonoxidative ATP generation and glycolytic enzyme cycling may be considerable.

Metabolic reaction rates by tracer kinetics. Rates of metabolic reactions also can be estimated by administering an MR-visible tracer and monitoring its rate of incorporation into tissue metabolites. ^{13}C-MRS is ideal for such studies because the relative lack of background signal attributed to the low natural abundance of ^{13}C leads to dramatic signal increases on metabolite ^{13}C-enrichment (Fig. 6). Furthermore, a wide range of metabolic products can be monitored and both positional and isotopic enrichment data can be determined, which offers a significant advantage over mass spectrometry. The simplest labeling strategies monitor the accumulation of tracer into macronutrient pools. Glycogen synthesis can be readily detected in muscle and liver using labeled glucose, and insulin-stimulated muscle glycogen synthesis has been found to be decreased in type 2 diabetes (82). Similarly, postprandial liver glycogen synthesis is decreased in type 2 diabetic patients, accompanied by impaired suppression of endogenous glucose production (83). Patients with poorly controlled type 1 diabetes also have impaired postprandial hepatic glycogen synthesis (84). Ingestion of ^{13}C-labeled fatty acids allows postprandial fat storage in liver and muscle to be determined, and both were found to be elevated in type 2 diabetes (85). More complex pulse-chase experiments (tracer administration followed by nonlabeled washout) enable metabolite synthesis and degradation (e.g., of liver glycogen) to be concurrently monitored. This style of study has surprisingly demonstrated that glycogen turnover occurs in liver in both fed and fasting states (86) and in muscle during steady-state exercise (87). Infusion of multiple ^{13}C-labeled tracers has permitted the relative contributions of different glucose sources to liver glycogen repletion to be determined under fed and fasting conditions (70).

Sophisticated computer-modeling techniques enable more complex metabolic reaction schemes to be assessed. Rates of oxidation via the tricarboxylic acid (TCA) cycle can be estimated in muscle by using [2-^{13}C]acetate as a precursor substrate and monitoring the rate of enrichment of the muscle glutamate pool, which acts as a surrogate for the intermediates of the TCA cycle (81). Decreased muscle substrate oxidation was found in two insulin-resistant cohorts of subjects (healthy older adults [77] and offspring of type 2 diabetic patients [88]), demonstrating an association between peripheral mitochondrial function and insulin sensitivity. Conversely, increased substrate oxidation rates have been observed in endurance-trained individuals (78).

Using [1-^{13}C]glucose as a substrate, multiple reaction rates can be measured in brain, including the TCA cycle flux, α-ketogutarate/glutamate exchange, and a unique metabolic parameter, the rate of excitatory neurotransmitter (glutamate/glutamine) cycling between neuron and astrocyte (89,90). Glial contributions to these cerebral metabolic rates can be estimated with [2-^{13}C]acetate as the metabolic precursor because of the preferential uptake by astrocytes (91). With multivoxel data acquisition plus segmentation analyses, gray- and white-matter compartmentation also can be resolved (92). Significant increases in TCA cycle oxidation rates have been observed in the visual cortex in response to visual stimulation using direct (93) and indirect (94) techniques to measure ^{13}C isotopic labeling. In contrast, neurotransmitter cycling, TCA cycle flux, and glucose oxidation were found to be decreased in Alzheimer's disease (95) and healthy aging (96). Abnormalities in brain glucose metabolism also have been observed in other mitochondrial and metabolic disorders (97). More recently, plasma lactate has emerged as a significant substrate source for brain metabolism (98).

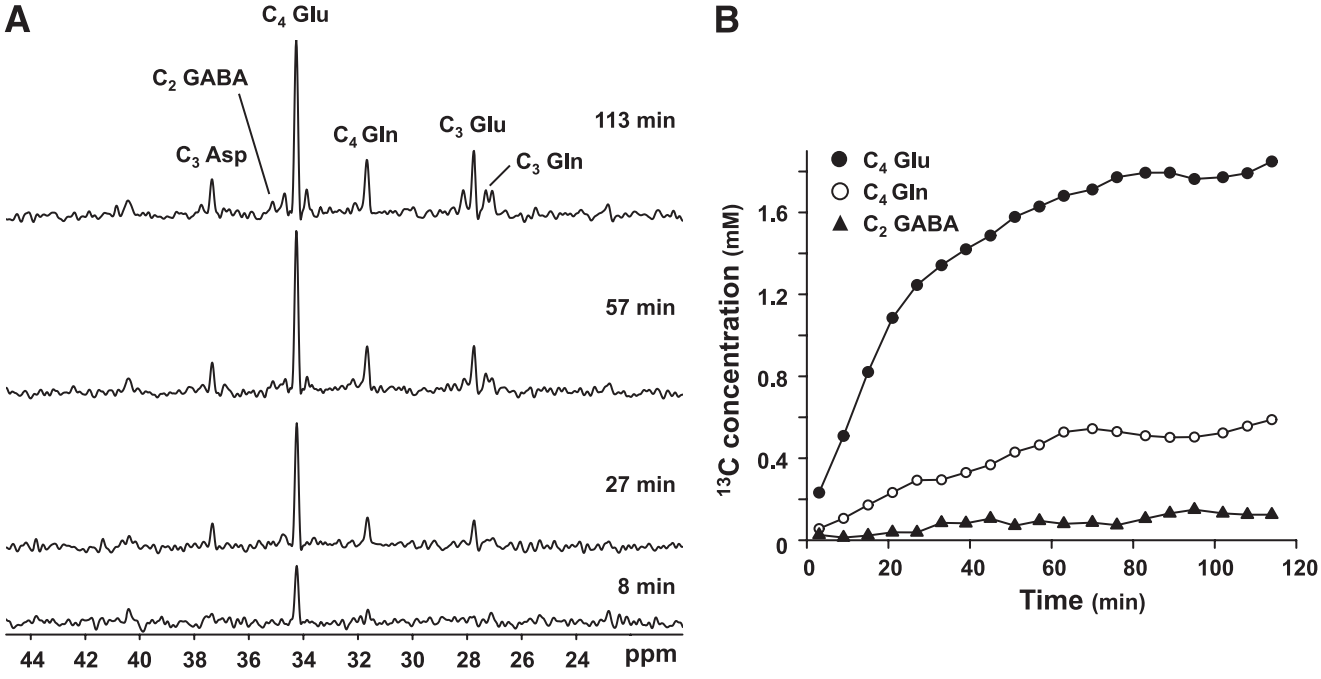

FIG. 6. Reaction rates can be assessed using ^{13}C tracer kinetics. In the brain, intravenous infusion of 1-^{13}C glucose leads to positional enrichment of several cerebral metabolites (*A*), including glutamate (Glu), glutamine (Gln), aspartate (Asp), and GABA. Metabolic modeling of the timecourses of enrichment (*B*) (●, C_4-Glu; ○, C_4-Gln; ▲, C_2-GABA) yields estimated reaction rates (e.g., TCA cycle flux, neurotransmitter cycling).

MULTIPARAMETER MRS STUDIES

One of the most powerful aspects of using MRS to study metabolism in vivo is that multiple independent parameters of metabolic function can be assessed across a range of tissues. This capability offers a unique ability to explore the mechanistic basis for the pathogenesis of metabolic diseases and/or syndromes. MRS studies were a key factor in elucidating the role of glucose transport in the mechanism of muscle insulin resistance in type 2 diabetes. Insulin-stimulated rates of muscle glycogen synthesis (82), measured by ^{13}C-MRS, were found to be attenuated in type 2 diabetes. Crucially, ^{31}P-MRS studies demonstrated that there also was a blunted increase in the intracellular concentration of glucose-6-phosphate in diabetic muscle, consistent with impaired glucose transport/phosphorylation activity, rather than a defect in glycogen synthase activity (99).

Using a multinuclear approach, a relationship between peripheral lipid deposition, muscle bioenergetics, and insulin resistance also has been demonstrated. In two cohorts of insulin-resistant subjects (76,77,88), the accumulation of IMCL (and IHL in [76]), measured by localized ^{1}H-MRS, was associated with decreases in substrate oxidation (TCA cycle flux) and rates of $P_i \rightarrow$ ATP flux in resting muscle, determined using dynamic ^{13}C-MRS and ^{31}P-saturation-transfer MRS, respectively. These studies suggest that a decline in basal mitochondrial activity, corroborated using two independent MRS biomarkers of mitochondrial metabolism, may play a role in the pathogenesis of peripheral insulin resistance and the development of type 2 diabetes. More recently, postprandial macronutrient storage in muscle and liver in response to a carbohydrate meal has been examined using ^{1}H-MRS to measure lipid accumulation and ^{13}C-MRS to assess glycogen synthesis (100). Muscle insulin resistance alters the partitioning of carbohydrate away from muscle glycogen synthesis and toward hepatic lipogenesis.

Interleaved ^{31}P/^{1}H-MRS techniques allow muscle HEP metabolism and myoglobin deoxygenation to be assessed simultaneously during exercise or ischemia (101) and have revealed complex interactions between vascular function, intracellular oxygenation, and mitochondrial function in elite athletes (102).

FUTURE DIRECTIONS FOR IN VIVO MRS

There is continuous development of novel MRS hardware, pulses, sequences, and techniques to improve the investigation of human metabolism in vivo. These occur in concert with a continual shift toward higher magnetic field strengths, which is accompanied by increased signal, wider spectral bandwidth, and enhanced spectral resolution. However, elevated power requirements at higher fields may lead to excessive localized power deposition, particularly for high-duty cycle sequences and those involving decoupling. The increased acoustic noise and space confinement of these systems may also impact subject tolerance. In this section, we highlight a few areas of development that already are generating significant interest.

Functional and metabolic heterogeneity is apparent not just between organs but also within a single tissue. Muscle HEP content is dependent on fiber type (24), and variations in IMCL distribution (103,104) and Pi → ATP flux (105) have been observed in different muscle of the calf. Differences in metabolite content and reaction rates are also apparent between regions of the brain and between gray matter, white matter, and cerebrospinal fluid (92,106). To robustly investigate metabolism in vivo, localized or spatially mapped versions of many of the techniques mentioned in this article are required. Spectroscopic imaging (SI) methods, which obtain MR spectra on a point-by-point basis across an entire region of interest, offer an attractive methodology by which this can be accomplished (Fig. 7), and certain applications already have begun to benefit from this approach (104,106–108). The recent development of multichannel detection coils augments the SI approach, concomitantly enhancing spatial coverage and decreasing scan time.

Adipose tissue has been studied in a limited manner with MRS but suffers from severe spectral broadening as a result of the short T_2 relaxation times of lipid. However, the metabolic significance of regional differences in glucose and fat metabolism between visceral and subcutaneous fat compartments, and recent studies demonstrating the existence of subclavicular brown fat in humans, is beginning to spur MRS investigation of these tissues.

MR methodology lacks a direct technique to investigate oxygen metabolism in vivo. Recently, ^{17}*O*-MRS has been implemented in animal models to measure cerebral blood flow and the metabolic rate of oxygen consumption during $^{17}O_2$ inhalation. Cerebral oxygen consumption was found to increase in the visual cortex with visual stimulation and agreed well with ^{31}P-MRS–determined rates of ATP synthesis (109), suggesting that this technique could successfully be translated to human research.

Despite its vast potential, ^{13}C-MRS is inherently limited by low signal/noise and a broad chemical shift range. Two approaches that enhance the sensitivity of ^{13}C measurements may transform its applicability to metabolic studies. Proton-observe/carbon-edited (POCE) techniques acquire ^{1}H-spectra but "edit" the spectrum to select protons coupled to ^{13}C nuclei (Fig. 8). Using this method, ^{13}C-enrichment data can be obtained with the superior localization accuracy and enhanced sensitivity of ^{1}H-MRS. In vivo, the application of POCE has been restricted by the relatively narrow bandwidth and spectral resolution of ^{1}H-MRS, but the availability of high-field systems may overcome this restriction, providing high-quality shimming routines ensure sufficient spectral resolution (110). Hyperpolarization favorably alters the Boltzmann distribution of ^{13}C spins in a target molecule, increasing sensitivity by several orders of magnitude, such that hyperpolarized ^{13}C-tracers can be observed with a single scan. Current applications are limited because of the requirement for specialized equipment,

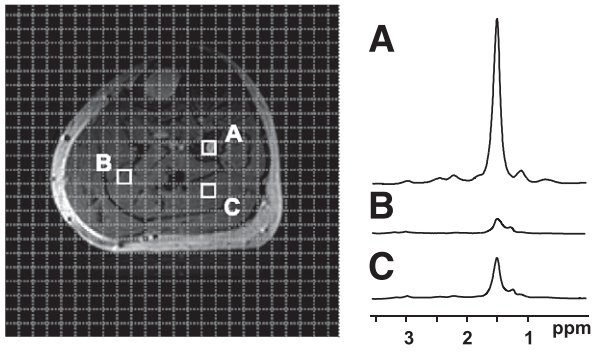

FIG. 7. Magnetic resonance spectroscopic imaging (MRSI) techniques enable the acquisition of spectral data on a point-by-point basis across a region of interest. Muscle ^{1}H-MRSI reveals distinct differences in lipid content between bone marrow (voxel A) and two different locations in the soleus (voxels B and C).

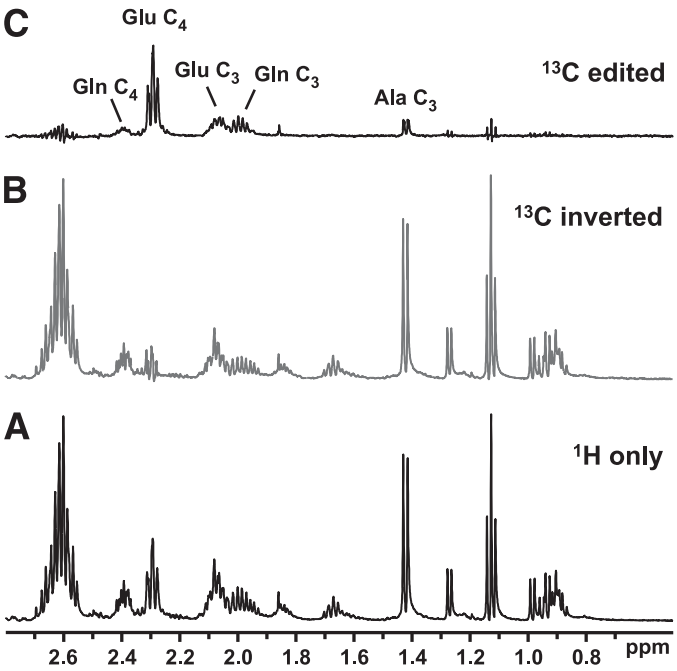

FIG. 8. POCE MRS can be used to enhance the detection of ^{13}C-enriched metabolites. *A*: Standard ^{1}H acquisition. *B*: The incorporation of an additional ^{13}C pulse in the ^{1}H pulse sequence selectively inverts the signal of all ^{1}H bound to ^{13}C; ^{1}H bound to ^{12}C are unaffected. *C*: The difference spectrum (*A* minus *B*) yields only ^{13}C-enriched metabolites. Fractional enrichment can be calculated from the ratio of *C*-to-*A*. These example spectra from a muscle extract show ^{13}C enrichment at multiple sites, including the C_4 and C_3 positions of glutamate (Glu) and glutamine (Gln) and C_3-alanine (Ala).

the limited number of metabolic substrates, and the extremely short lifetimes of hyperpolarized ^{13}C. Nonetheless, in vivo studies have been performed in animal models to investigate the rapid metabolic fluxes of pyruvate (111) and lactate (112). Broader metabolic applications are yet to be developed, but this technique may potentially revolutionize in vivo ^{13}C-MRS.

Chemical-exchange-saturation-transfer (CEST) is an MT method that examines generic exchange between labile metabolite protons and bulk water. Although primarily implemented as an MRI-based technique that provides exchange-based contrast, several intriguing metabolic applications are emerging. These include pH imaging (e.g., to discern tumors), glucose sensing, and imaging of glycogen distribution. CEST may also have applications as a biomarker of gene expression detecting ^{1}H exchange fluxes that are catalyzed by a specific enzyme, a gene delivery agent or by the RNA polymer itself. The review by Zhou and van Zijl (113) provides a comprehensive analysis of CEST techniques.

To date, the capabilities of MRS primarily have been exploited in research where it has advanced our understanding of the mechanisms behind fundamental metabolic processes and the pathogenesis of disease. More widespread availability and the translation of MRS into a practical clinical diagnostic tool has been curtailed by several factors: dedicated spectroscopy systems and specialized expertise have been required leading to high costs, scan times are relatively long, and many individuals are excluded from undergoing MR scans (e.g., those with implanted metal, pacemakers, or claustrophobia). However, the new generation of high-field (3 Tesla, and above) clinical MRI scanners can be equipped with spectroscopy capabilities, and this, combined with the advent of robust automated processing routines and rapid data-acquisition techniques, offers the scope for more widespread application of MRS techniques to human research and the potential for translation into a clinically useful methodology. In vivo MRS promises to be a key technique contributing to the investigation of human metabolism in the 21st century.

ACKNOWLEDGEMENTS

No potential conflicts of interest relevant to this article were reported.

D.E.B. and G.I.S. wrote the manuscript.

REFERENCES

1. de Graaf RA. *In Vivo NMR Spectroscopy: Principles and Techniques*. Chichester, Wiley, 2008
2. Boesch C, Slotboom J, Hoppeler H, Kreis R. In vivo determination of intra-myocellular lipids in human muscle by means of localized ^{1}H-MR-spectroscopy. Magn Reson Med 1997;37:484–493
3. Krssak M, Falk Petersen K, Dresner A, et al. Intramyocellular lipid concentrations are correlated with insulin sensitivity in humans: a ^{1}H NMR spectroscopy study. Diabetologia 1999;42:113–116
4. Machann J, Stefan N, Schick F. (1)H MR spectroscopy of skeletal muscle, liver and bone marrow. Eur J Radiol 2008;67:275–284
5. Szczepaniak LS, Babcock EE, Schick F, et al. Measurement of intracellular triglyceride stores by H spectroscopy: validation in vivo. Am J Physiol 1999;276:E977–E989
6. van Loon LJ, Koopman R, Manders R, van der Weegen W, van Kranenburg GP, Keizer HA. Intramyocellular lipid content in type 2 diabetes patients compared with overweight sedentary men and highly trained endurance athletes. Am J Physiol Endocrinol Metab 2004;287:E558–E565
7. Savage DB, Petersen KF, Shulman GI. Disordered lipid metabolism and the pathogenesis of insulin resistance. Physiol Rev 2007;87:507–520
8. Shulman GI. Cellular mechanisms of insulin resistance. J Clin Invest 2000;106:171–176
9. Liu L, Zhang Y, Chen N, Shi X, Tsang B, Yu YH. Upregulation of myocellular DGAT1 augments triglyceride synthesis in skeletal muscle and protects against fat-induced insulin resistance. J Clin Invest 2007;117:1679–1689
10. Schenk S, Horowitz JF. Acute exercise increases triglyceride synthesis in skeletal muscle and prevents fatty acid-induced insulin resistance. J Clin Invest 2007;117:1690–1698
11. Seppälä-Lindroos A, Vehkavaara S, Häkkinen AM, et al. Fat accumulation in the liver is associated with defects in insulin suppression of glucose production and serum free fatty acids independent of obesity in normal men. J Clin Endocrinol Metab 2002;87:3023–3028
12. Petersen KF, Oral EA, Dufour S, et al. Leptin reverses insulin resistance and hepatic steatosis in patients with severe lipodystrophy. J Clin Invest 2002;109:1345–1350
13. Mayerson AB, Hundal RS, Dufour S, et al. The effects of rosiglitazone on insulin sensitivity, lipolysis, and hepatic and skeletal muscle triglyceride content in patients with type 2 diabetes. Diabetes 2002;51:797–802
14. DeFronzo RA, Goodman AM; The Multicenter Metformin Study Group. Efficacy of metformin in patients with non-insulin-dependent diabetes mellitus. N Engl J Med 1995;333:541–549
15. Thamer C, Machann J, Stefan N, et al. High visceral fat mass and high liver fat are associated with resistance to lifestyle intervention. Obesity (Silver Spring) 2007;15:531–538
16. Larson-Meyer DE, Newcomer BR, Heilbronn LK, et al.; Pennington CALERIE Team. Effect of 6-month calorie restriction and exercise on serum and liver lipids and markers of liver function. Obesity (Silver Spring) 2008;16:1355–1362
17. Petersen KF, Dufour S, Befroy D, Lehrke M, Hendler RE, Shulman GI. Reversal of nonalcoholic hepatic steatosis, hepatic insulin resistance, and hyperglycemia by moderate weight reduction in patients with type 2 diabetes. Diabetes 2005;54:603–608
18. Machann J, Thamer C, Stefan N, et al. Follow-up whole-body assessment of adipose tissue compartments during a lifestyle intervention in a large cohort at increased risk for type 2 diabetes. Radiology 2010;257:353–363
19. Browning JD, Szczepaniak LS, Dobbins R, et al. Prevalence of hepatic steatosis in an urban population in the United States: impact of ethnicity. Hepatology 2004;40:1387–1395

20. Petersen KF, Dufour S, Feng J, et al. Increased prevalence of insulin resistance and nonalcoholic fatty liver disease in Asian-Indian men. Proc Natl Acad Sci USA 2006;103:18273–18277
21. den Hollander JA, Evanochko WT, Pohost GM. Observation of cardiac lipids in humans by localized ^{1}H magnetic resonance spectroscopic imaging. Magn Reson Med 1994;32:175–180
22. Reingold JS, McGavock JM, Kaka S, Tillery T, Victor RG, Szczepaniak LS. Determination of triglyceride in the human myocardium by magnetic resonance spectroscopy: reproducibility and sensitivity of the method. Am J Physiol Endocrinol Metab 2005;289:E935–E939
23. McGavock JM, Lingvay I, Zib I, et al. Cardiac steatosis in diabetes mellitus: a ^{1}H-magnetic resonance spectroscopy study. Circulation 2007;116:1170–1175
24. Meyer RA, Brown TR, Kushmerick MJ. Phosphorus nuclear magnetic resonance of fast- and slow-twitch muscle. Am J Physiol 1985;248:C279–C287
25. Barnes PR, Kemp GJ, Taylor DJ, Radda GK. Skeletal muscle metabolism in myotonic dystrophy A ^{31}P magnetic resonance spectroscopy study. Brain 1997;120:1699–1711
26. Conway MA, Allis J, Ouwerkerk R, Niioka T, Rajagopalan B, Radda GK. Detection of low phosphocreatine to ATP ratio in failing hypertrophied human myocardium by ^{31}P magnetic resonance spectroscopy. Lancet 1991;338:973–976
27. Neubauer S, Krahe T, Schindler R, et al. ^{31}P magnetic resonance spectroscopy in dilated cardiomyopathy and coronary artery disease: altered cardiac high-energy phosphate metabolism in heart failure. Circulation 1992;86:1810–1818
28. Beer M. Cardiac spectroscopy: techniques, indications and clinical results. Eur Radiol 2004;14:1034–1047
29. Neubauer S, Horn M, Cramer M, et al. Myocardial phosphocreatine-to-ATP ratio is a predictor of mortality in patients with dilated cardiomyopathy. Circulation 1997;96:2190–2196
30. Nakae I, Mitsunami K, Matsuo S, Horie M. Creatine depletion and altered fatty acid metabolism in diseased human hearts: clinical investigation using ^{1}H magnetic resonance spectroscopy and ^{123}I BMIPP myocardial scintigraphy. Acta Radiol 2007;48:436–443
31. Nakae I, Mitsunami K, Matsuo S, et al. Myocardial creatine concentration in various nonischemic heart diseases assessed by ^{1}H magnetic resonance spectroscopy. Circ J 2005;69:711–716
32. Bottomley PA, Weiss RG. Non-invasive magnetic-resonance detection of creatine depletion in non-viable infarcted myocardium. Lancet 1998;351:714–718
33. Diamant M, Lamb HJ, Groeneveld Y, et al. Diastolic dysfunction is associated with altered myocardial metabolism in asymptomatic normotensive patients with well-controlled type 2 diabetes mellitus. J Am Coll Cardiol 2003;42:328–335
34. Nair S, P Chacko V, Arnold C, Diehl AM. Hepatic ATP reserve and efficiency of replenishing: comparison between obese and nonobese normal individuals. Am J Gastroenterol 2003;98:466–470
35. Szendroedi J, Chmelik M, Schmid AI, et al. Abnormal hepatic energy homeostasis in type 2 diabetes. Hepatology 2009;50:1079–1086
36. Khan SA, Cox IJ, Hamilton G, Thomas HC, Taylor-Robinson SD. In vivo and in vitro nuclear magnetic resonance spectroscopy as a tool for investigating hepatobiliary disease: a review of H and P MRS applications. Liver Int 2005;25:273–281
37. Lim AK, Patel N, Hamilton G, Hajnal JV, Goldin RD, Taylor-Robinson SD. The relationship of in vivo ^{31}P MR spectroscopy to histology in chronic hepatitis C. Hepatology 2003;37:788–794
38. Norén B, Lundberg P, Ressner M, Wirell S, Almer S, Smedby O. Absolute quantification of human liver metabolite concentrations by localized in vivo ^{31}P NMR spectroscopy in diffuse liver disease. Eur Radiol 2005;15:148–157
39. Graham GD, Blamire AM, Rothman DL, et al. Early temporal variation of cerebral metabolites after human stroke: a proton magnetic resonance spectroscopy study. Stroke 1993;24:1891–1896
40. Hetherington HP, Pan JW, Spencer DD. ^{1}H and ^{31}P spectroscopy and bioenergetics in the lateralization of seizures in temporal lobe epilepsy. J Magn Reson Imaging 2002;16:477–483
41. Rothman DL, Petroff OA, Behar KL, Mattson RH. Localized ^{1}H NMR measurements of gamma-aminobutyric acid in human brain in vivo. Proc Natl Acad Sci USA 1993;90:5662–5666
42. Petroff OA, Behar KL, Mattson RH, Rothman DL. Human brain gamma-aminobutyric acid levels and seizure control following initiation of vigabatrin therapy. J Neurochem 1996;67:2399–2404
43. Prompers JJ, Jeneson JA, Drost MR, Oomens CC, Strijkers GJ, Nicolay K. Dynamic MRS and MRI of skeletal muscle function and biomechanics. NMR Biomed 2006;19:927–953
44. Arnold DL, Matthews PM, Radda GK. Metabolic recovery after exercise and the assessment of mitochondrial function in vivo in human skeletal muscle by means of ^{31}P NMR. Magn Reson Med 1984;1:307–315
45. Larson-Meyer DE, Newcomer BR, Hunter GR, Hetherington HP, Weinsier RL. ^{31}P MRS measurement of mitochondrial function in skeletal muscle: reliability, force-level sensitivity and relation to whole body maximal oxygen uptake. NMR Biomed 2000;13:14–27
46. Hunter GR, Newcomer BR, Larson-Meyer DE, Bamman MM, Weinsier RL. Muscle metabolic economy is inversely related to exercise intensity and type II myofiber distribution. Muscle Nerve 2001;24:654–661
47. Kent-Braun JA. Skeletal muscle fatigue in old age: whose advantage? Exerc Sport Sci Rev 2009;37:3–9
48. Lanza IR, Befroy DE, Kent-Braun JA. Age-related changes in ATP-producing pathways in human skeletal muscle in vivo. J Appl Physiol 2005;99:1736–1744
49. Massie BM, Conway M, Yonge R, et al. ^{31}P nuclear magnetic resonance evidence of abnormal skeletal muscle metabolism in patients with congestive heart failure. Am J Cardiol 1987;60:309–315
50. Esterhammer R, Schocke M, Gorny O, et al. Phosphocreatine kinetics in the calf muscle of patients with bilateral symptomatic peripheral arterial disease during exhaustive incremental exercise. Mol Imaging Biol 2008;10:30–39
51. Barnes PR, Taylor DJ, Kemp GJ, Radda GK. Skeletal muscle bioenergetics in the chronic fatigue syndrome. J Neurol Neurosurg Psychiatry 1993;56:679–683
52. Scheuermann-Freestone M, Madsen PL, Manners D, et al. Abnormal cardiac and skeletal muscle energy metabolism in patients with type 2 diabetes. Circulation 2003;107:3040–3046
53. Weiss RG, Bottomley PA, Hardy CJ, Gerstenblith G. Regional myocardial metabolism of high-energy phosphates during isometric exercise in patients with coronary artery disease. N Engl J Med 1990;323:1593–1600
54. Yabe T, Mitsunami K, Okada M, Morikawa S, Inubushi T, Kinoshita M. Detection of myocardial ischemia by ^{31}P magnetic resonance spectroscopy during handgrip exercise. Circulation 1994;89:1709–1716
55. Buchthal SD, den Hollander JA, Merz CN, et al. Abnormal myocardial phosphorus-31 nuclear magnetic resonance spectroscopy in women with chest pain but normal coronary angiograms. N Engl J Med 2000;342:829–835
56. Wang ZY, Noyszewski EA, Leigh JS Jr. In vivo MRS measurement of deoxymyoglobin in human forearms. Magn Reson Med 1990;14:562–567
57. Molé PA, Chung Y, Tran TK, Sailasuta N, Hurd R, Jue T. Myoglobin desaturation with exercise intensity in human gastrocnemius muscle. Am J Physiol 1999;277:R173–R180
58. Wigmore DM, Befroy DE, Lanza IR, Kent-Braun JA. Contraction frequency modulates muscle fatigue and the rate of myoglobin desaturation during incremental contractions in humans. Appl Physiol Nutr Metab 2008;33:915–921
59. Kreis R, Bruegger K, Skjelsvik C, et al. Quantitative (1)H magnetic resonance spectroscopy of myoglobin de- and reoxygenation in skeletal muscle: reproducibility and effects of location and disease. Magn Reson Med 2001;46:240–248
60. Meyerspeer M, Kemp GJ, Mlynárik V, et al. Direct noninvasive quantification of lactate and high energy phosphates simultaneously in exercising human skeletal muscle by localized magnetic resonance spectroscopy. Magn Reson Med 2007;57:654–660
61. Pan JW, Hamm JR, Hetherington HP, Rothman DL, Shulman RG. Correlation of lactate and pH in human skeletal muscle after exercise by ^{1}H NMR. Magn Reson Med 1991;20:57–65
62. Prichard J, Rothman D, Novotny E, et al. Lactate rise detected by ^{1}H NMR in human visual cortex during physiologic stimulation. Proc Natl Acad Sci USA 1991;88:5829–5831
63. Price TB, Rothman DL, Avison MJ, Buonamico P, Shulman RG. ^{13}C-NMR measurements of muscle glycogen during low-intensity exercise. J Appl Physiol 1991;70:1836–1844
64. Price TB, Rothman DL, Shulman RG. NMR of glycogen in exercise. Proc Nutr Soc 1999;58:851–859
65. Brechtel K, Niess AM, Machann J, et al. Utilisation of intramyocellular lipids (IMCLs) during exercise as assessed by proton magnetic resonance spectroscopy (^{1}H-MRS). Horm Metab Res 2001;33:63–66
66. Rothman DL, Magnusson I, Katz LD, Shulman RG, Shulman GI. Quantitation of hepatic glycogenolysis and gluconeogenesis in fasting humans with ^{13}C NMR. Science 1991;254:573–576
67. Stannard SR, Thompson MW, Fairbairn K, Huard B, Sachinwalla T, Thompson CH. Fasting for 72 h increases intramyocellular lipid content in nondiabetic, physically fit men. Am J Physiol Endocrinol Metab 2002;283:E1185–E1191
68. Moller L, Stodkilde-Jorgensen H, Jensen FT, Jorgensen JO. Fasting in healthy subjects is associated with intrahepatic accumulation of lipids as

assessed by ^{1}H-magnetic resonance spectroscopy. Clin Sci (Lond) 2008;114:547–552
69. Jue T, Rothman DL, Tavitian BA, Shulman RG. Natural-abundance ^{13}C NMR study of glycogen repletion in human liver and muscle. Proc Natl Acad Sci USA 1989;86:1439–1442
70. Shulman GI, Cline G, Schumann WC, Chandramouli V, Kumaran K, Landau BR. Quantitative comparison of pathways of hepatic glycogen repletion in fed and fasted humans. Am J Physiol 1990;259:E335–E341
71. Taylor R, Magnusson I, Rothman DL, et al. Direct assessment of liver glycogen storage by ^{13}C nuclear magnetic resonance spectroscopy and regulation of glucose homeostasis after a mixed meal in normal subjects. J Clin Invest 1996;97:126–132
72. Petersen KF, Price T, Cline GW, Rothman DL, Shulman GI. Contribution of net hepatic glycogenolysis to glucose production during the early postprandial period. Am J Physiol 1996;270:E186–E191
73. Magnusson I, Rothman DL, Katz LD, Shulman RG, Shulman GI. Increased rate of gluconeogenesis in type II diabetes mellitus: a ^{13}C nuclear magnetic resonance study. J Clin Invest 1992;90:1323–1327
74. Weiss RG, Gerstenblith G, Bottomley PA. ATP flux through creatine kinase in the normal, stressed, and failing human heart. Proc Natl Acad Sci USA 2005;102:808–813
75. Smith CS, Bottomley PA, Schulman SP, Gerstenblith G, Weiss RG. Altered creatine kinase adenosine triphosphate kinetics in failing hypertrophied human myocardium. Circulation 2006;114:1151–1158
76. Petersen KF, Befroy D, Dufour S, et al. Mitochondrial dysfunction in the elderly: possible role in insulin resistance. Science 2003;300:1140–1142
77. Petersen KF, Dufour S, Befroy D, Garcia R, Shulman GI. Impaired mitochondrial activity in the insulin-resistant offspring of patients with type 2 diabetes. N Engl J Med 2004;350:664–671
78. Befroy DE, Petersen KF, Dufour S, Mason GF, Rothman DL, Shulman GI. Increased substrate oxidation and mitochondrial uncoupling in skeletal muscle of endurance-trained individuals. Proc Natl Acad Sci USA 2008;105:16701–16706
79. Lei H, Ugurbil K, Chen W. Measurement of unidirectional Pi to ATP flux in human visual cortex at 7 T by using in vivo ^{31}P magnetic resonance spectroscopy. Proc Natl Acad Sci USA 2003;100:14409–14414
80. Schmid AI, Chmelík M, Szendroedi J, et al. Quantitative ATP synthesis in human liver measured by localized ^{31}P spectroscopy using the magnetization transfer experiment. NMR Biomed 2008;21:437–443
81. Befroy DE, Falk Petersen K, Rothman DL, Shulman GI. Assessment of in vivo mitochondrial metabolism by magnetic resonance spectroscopy. Methods Enzymol 2009;457:373–393
82. Shulman GI, Rothman DL, Jue T, Stein P, DeFronzo RA, Shulman RG. Quantitation of muscle glycogen synthesis in normal subjects and subjects with non-insulin-dependent diabetes by ^{13}C nuclear magnetic resonance spectroscopy. N Engl J Med 1990;322:223–228
83. Krssak M, Brehm A, Bernroider E, et al. Alterations in postprandial hepatic glycogen metabolism in type 2 diabetes. Diabetes 2004;53:3048–3056
84. Hwang JH, Perseghin G, Rothman DL, et al. Impaired net hepatic glycogen synthesis in insulin-dependent diabetic subjects during mixed meal ingestion. A ^{13}C nuclear magnetic resonance spectroscopy study. J Clin Invest 1995;95:783–787
85. Ravikumar B, Carey PE, Snaar JE, et al. Real-time assessment of postprandial fat storage in liver and skeletal muscle in health and type 2 diabetes. Am J Physiol Endocrinol Metab 2005;288:E789–E797
86. Magnusson I, Rothman DL, Jucker B, Cline GW, Shulman RG, Shulman GI. Liver glycogen turnover in fed and fasted humans. Am J Physiol 1994;266:E796–E803
87. Price TB, Taylor R, Mason GF, Rothman DL, Shulman GI, Shulman RG. Turnover of human muscle glycogen with low-intensity exercise. Med Sci Sports Exerc 1994;26:983–991
88. Befroy DE, Petersen KF, Dufour S, et al. Impaired mitochondrial substrate oxidation in muscle of insulin-resistant offspring of type 2 diabetic patients. Diabetes 2007;56:1376–1381
89. Mason GF, Gruetter R, Rothman DL, Behar KL, Shulman RG, Novotny EJ. Simultaneous determination of the rates of the TCA cycle, glucose utilization, alpha-ketoglutarate/glutamate exchange, and glutamine synthesis in human brain by NMR. J Cereb Blood Flow Metab 1995;15:12–25
90. Shen J, Petersen KF, Behar KL, et al. Determination of the rate of the glutamate/glutamine cycle in the human brain by in vivo ^{13}C NMR. Proc Natl Acad Sci USA 1999;96:8235–8240
91. Lebon V, Petersen KF, Cline GW, et al. Astroglial contribution to brain energy metabolism in humans revealed by ^{13}C nuclear magnetic resonance spectroscopy: elucidation of the dominant pathway for neurotransmitter glutamate repletion and measurement of astrocytic oxidative metabolism. J Neurosci 2002;22:1523–1531
92. Mason GF, Pan JW, Chu WJ, et al. Measurement of the tricarboxylic acid cycle rate in human grey and white matter in vivo by ^{1}H-[^{13}C] magnetic resonance spectroscopy at 4.1T. J Cereb Blood Flow Metab 1999;19:1179–1188
93. Chhina N, Kuestermann E, Halliday J, et al. Measurement of human tricarboxylic acid cycle rates during visual activation by (13)C magnetic resonance spectroscopy. J Neurosci Res 2001;66:737–746
94. Chen W, Zhu XH, Gruetter R, Seaquist ER, Adriany G, Ugurbil K. Study of tricarboxylic acid cycle flux changes in human visual cortex during hemifield visual stimulation using (1)H-[(13)C] MRS and fMRI. Magn Reson Med 2001;45:349–355
95. Lin AP, Shic F, Enriquez C, Ross BD. Reduced glutamate neurotransmission in patients with Alzheimer's disease: an in vivo (13)C magnetic resonance spectroscopy study. MAGMA 2003;16:29–42
96. Boumezbeur F, Mason GF, de Graaf RA, et al. Altered brain mitochondrial metabolism in healthy aging as assessed by in vivo magnetic resonance spectroscopy. J Cereb Blood Flow Metab 2010;30:211–221
97. Blüml S, Moreno A, Hwang JH, Ross BD. 1-(13)C glucose magnetic resonance spectroscopy of pediatric and adult brain disorders. NMR Biomed 2001;14:19–32
98. Boumezbeur F, Petersen KF, Cline GW, et al. The contribution of blood lactate to brain energy metabolism in humans measured by dynamic ^{13}C nuclear magnetic resonance spectroscopy. J Neurosci 2010;30:13983–13991
99. Rothman DL, Shulman RG, Shulman GI. ^{31}P nuclear magnetic resonance measurements of muscle glucose-6-phosphate: evidence for reduced insulin-dependent muscle glucose transport or phosphorylation activity in non-insulin-dependent diabetes mellitus. J Clin Invest 1992;89:1069–1075
100. Petersen KF, Dufour S, Savage DB, et al. The role of skeletal muscle insulin resistance in the pathogenesis of the metabolic syndrome. Proc Natl Acad Sci USA 2007;104:12587–12594
101. Vanderthommen M, Duteil S, Wary C, et al. A comparison of voluntary and electrically induced contractions by interleaved ^{1}H- and ^{31}P-NMRS in humans. J Appl Physiol 2003;94:1012–1024
102. Duteil S, Bourrilhon C, Raynaud JS, et al. Metabolic and vascular support for the role of myoglobin in humans: a multiparametric NMR study. Am J Physiol Regul Integr Comp Physiol 2004;287:R1441–R1449
103. Boesch C, Kreis R. Observation of intramyocellular lipids by ^{1}H-magnetic resonance spectroscopy. Ann N Y Acad Sci 2000;904:25–31
104. Vermathen P, Kreis R, Boesch C. Distribution of intramyocellular lipids in human calf muscles as determined by MR spectroscopic imaging. Magn Reson Med 2004;51:253–262
105. Befroy DE, Petersen KF, Shulman GI, Rothman DL. Localized ^{31}P saturation transfer reveals differences in gastrocnemius and soleus rates of ATP synthesis in-vivo. In *Proceedings of the International Society of Magnetic Resonance Medicine, Toronto, Canada, 2008*. Berkeley, CA, International Society of Magnetic Resonance Medicine, p. 2565
106. Hetherington HP, Mason GF, Pan JW, et al. Evaluation of cerebral gray and white matter metabolite differences by spectroscopic imaging at 4.1T. Magn Reson Med 1994;32:565–571
107. Pan JW, Stein DT, Telang F, et al. Spectroscopic imaging of glutamate C4 turnover in human brain. Magn Reson Med 2000;44:673–679
108. Weis J, Johansson L, Courivaud F, Karlsson FA, Ahlström H. Quantification of intramyocellular lipids in obese subjects using spectroscopic imaging with high spatial resolution. Magn Reson Med 2007;57:22–28
109. Zhu XH, Zhang N, Zhang Y, Uğurbil K, Chen W. New insights into central roles of cerebral oxygen metabolism in the resting and stimulus-evoked brain. J Cereb Blood Flow Metab 2009;29:10–18
110. de Graaf RA, Mason GF, Patel AB, Behar KL, Rothman DL. In vivo ^{1}H-[^{13}C]-NMR spectroscopy of cerebral metabolism. NMR Biomed 2003;16:339–357
111. Kohler SJ, Yen Y, Wolber J, et al. In vivo 13 carbon metabolic imaging at 3T with hyperpolarized ^{13}C-1-pyruvate. Magn Reson Med 2007;58:65–69
112. Chen AP, Kurhanewicz J, Bok R, et al. Feasibility of using hyperpolarized [1-^{13}C]lactate as a substrate for in vivo metabolic ^{13}C MRSI studies. Magn Reson Imaging 2008;26:721–726
113. Zhou J, van Zijl PCM. Chemical exchange saturation transfer imaging and spectroscopy. Prog Nucl Magn Reson Spectrosc 2006;48:109–136